journal

J. Am. Ceram. Soc., 98 [10] 3361–3366 (2015)
DOI: 10.1111/jace.13738

Radiation Stability of Spark-Plasma-Sintered Lead Vanadate Iodoapatite

Fengyuan Lu,[‡,†] Tiankai Yao,[§] Yaron Danon,[§] Jianren Zhou,[‡] Rodney C. Ewing,[¶] and Jie Lian[§,†]

[‡]Department of Mechanical and Industrial Engineering, Louisiana State University, Baton Rouge, Louisiana 70803

[§]Department of Mechanical, Aerospace, and Nuclear Engineering, Rensselaer Polytechnic Institute, Troy, New York 12180

[¶]Department of Geological & Environmental Sciences, Stanford University, Stanford, California 94305-2115

Spark-plasma-sintered lead vanadate iodoapatite $Pb_{9.85}(VO_4)_6I_{1.7}$, a promising nuclear waste form for the immobilization of I-129, was irradiated with energetic ions, electrons, and gamma rays, to investigate its radiation stability. *In situ* TEM observation of the 1 MeV Kr^{2+} irradiation shows that lead vanadate iodoapatite generally exhibits higher tolerance against ion irradiation-induced amorphization than lead vanadate fluorapatite, and the spark plasma sintering can further enhance its radiation stability attributed to the enhanced crystallinity, reduced defect concentration, and denser microstructure. The critical amorphization dose and critical temperature for the SPS-densified iodoapatite at 700°C are determined to be 0.25 dpa at room temperature and 230°C, respectively. No significant phase transformation or microstructural damage occurred under energetic electron and gamma irradiations. Raman spectra of gamma-ray-irradiated iodoapatite indicate improved V–O bond order at 500 kGy dose. Generally, the spark-plasma-sintered iodoapatite exhibits excellent radiation stability for nuclear waste form applications. The significantly enhanced radiation stability of the SPS-densified iodoapatite suggests that SPS holds great promise for fabricating iodoapatite waste form with minimum iodine loss and optimized radiation tolerance for effective management of highly volatile I-129.

I. Introduction

The management of radioactive wastes, particularly the long-lived actinides such as Pu, Np, and Am, and various types of fission products (FP) such as Cs-135, Sr-90, and I-129, is crucial to the development of safe nuclear energy. The volatile I-129 is a particularly troublesome FP due to its high mobility, volatility, and extremely long half-life of 15.7 million years, which requires a specially designed waste form for its long-term immobilization and disposal in geological repositories. The apatite structure-type $A^I_4A^{II}_6(BO_4)_6X_2$ (A^I, A^{II} = alkali, alkaline earths, rare earths, fission products, or actinides, B = Si, P, V, or Cr, and X = OH, O, or halogens) has an open-frame structure, in which six equivalent BO_4 tetrahedra are corner-connected to AO_6 metaprism columns to form one-dimensional tunnels that can accommodate large anionic species, such as iodine. Its high structural flexibility and excellent chemical durability make it a promising host phase for the immobilization of a wide range of radionuclides, especially the volatile I-129.[1–3] Extensive efforts have been made to effectively incorporate I-129[1,4–6] and several other FPs[7–9] and actinides[10–15] into the apatite structure for long-term geological disposal.

Lead vanadate iodoapatite $Pb_{10}(VO_4)_6I_2$, whose large A- and B-site atoms of Pb and V enable high loading of iodine anions in the tunnel, is a particularly suitable waste form candidate for the immobilization of I-129, along with other FPs and actinides. As a result, various experimental methods have been adopted to fabricate iodoapatite with purpose of improving I-129 waste management.[1,4,6,16,17] Due to the high mobility of iodine, the stability of the incorporated I-129 in the lead vanadate iodoapatite is of particular concern because the complex thermal and radiation environment of the waste form could potentially cause the release of I-129 to the surrounding environment. The iodine leaching rates in iodoapatite fabricated by conventional hot-pressing method were reported to be either higher than or comparable to AgI glass waste form.[18,19] Recently, a fabrication method combining low-temperature high-energy ball milling (HEBM) synthesis and spark plasma sintering (SPS) consolidation has been reported, which significantly reduces iodine loss during fabrication and greatly improves the thermal stability of the iodoapatite.[16,17] Specifically, as compared with previously reported methods, the HEBM synthesis method exhibits lower crystallization temperature, improved thermal stability, a higher decomposition temperature, and excellent iodine confinement for the iodoapatite.[16] The SPS consolidation further improves the thermal stability of the bulk iodoapatite, such that the structure remains highly stable up to a high temperature of 670°C, and the complete iodine loss does not occur until a very high temperature of 800°C is reached.[17]

The apatite-based nuclear waste form can incorporate a wide range of radionuclides including Pu-239, Am-241, Np-237, Sr-90, Tc-99, Cs-135, Cs-137, and I-129.[1,8,9,11,15] These radionuclides decay in different modes that generate energetic alpha-particles and alpha-recoils (in actinides), beta particles (in most FPs), and gamma rays (in FPs like I-129 and Cs-137), which can create complex radiation environments in the waste form. Considering the extremely long period required for geological disposition, the accumulation of radiation damage could potentially amorphize iodoapatite, reduce its durability and cause the release of the incorporated radionuclides,[20] particularly the volatile I-129. Therefore, the radiation tolerance of iodoapatite must be carefully evaluated. The radiation stability of various apatite compositions has been investigated previously, including natural F-rich apatite,[21] oxyapatite,[22–24] hydroxyapatite,[25] and fluorapatite.[25–27] However, the radiation stability of the I-129-bearing iodoapatite waste form has not been investigated. In this work, systematic irradiation experiments on the HEBM-synthesized and SPS-densified iodoapatite samples were performed to simulate the radiation effects caused by alpha, beta, and gamma decays, and the phase stability of the samples under the different radiation conditions was studied for evaluating their long-term performance as nuclear waste forms. The results show significantly enhanced radiation sta-

W. E. Lee—contributing editor

Manuscript No. 36582. Received March 17, 2015; approved May 31, 2015.
[†]Authors to whom correspondence should be addressed. e-mails: luf@lsu.edu and lianj@rpi.edu

bility in SPS-densified iodoapatite, indicating that SPS holds great promise for optimizing the fabrication of iodoapatite waste form with minimum iodine loss and maximized radiation tolerance.

II. Experimental Procedure

(1) Sample Preparation

Iodoapatite powders were prepared using low temperature (~50°C) HEBM-induced solid-state synthesis in a Fritsch Pulverisette 7 Premium Line planetary ball mill, as described in a previous report.[16] The starting powder ingredients of PbI_2, PbO, and V_2O_5 were ball-milled by 2-mm-sized ZrO_2 balls at 500 rpm for 20 h to form iodoapatite $Pb_{9.85}(VO_4)_6I_{1.7}$, which has a minor iodine deficiency and hence a slight deviation from the ideal stoichiometry of $Pb_{10}(VO_4)_6I_2$. The as-milled iodoapatite samples existed in the form of nanocrystals, mostly 4–10 nm in size, embedded in an amorphous matrix. The subsequent 1-hour heat treatment at 300°C resulted in a significant crystallization of the amorphous matrix and grain coarsening to 30–50 nm in size [shown in Fig. 1(a)], which exhibits a high iodine loading (>8 wt%) and greatly improved thermal stability, as compared with conventionally high-temperature-sintered iodoapatite.[1,18,19,28] This ball-milled and heat-treated sample is denoted by BM-300C. Consolidation of the thermally treated iodoapatite powders was achieved by SPS with a very high heating rate of 200°C/min and a short temperature holding time of 1 min at the maximum temperature of 700°C,[17] and the consolidated sample is denoted by SPS-700C. Such a fast heating rate and short sintering duration enable the maintenance of the chemical composition and structure of the lead vanadate apatite without iodine loss, which usually occurs at this high-temperature range.

(2) Irradiation Experiments

The irradiations of the iodoapatite samples were carried out in three different ways: energetic ion irradiation, electron irradiation, and gamma ray irradiation. Energetic 1 MeV Kr^{2+} irradiation was utilized to simulate the radiation damage caused by the alpha decay events of the incorporated actinides in apatite waste forms. Generally, alpha decay is the radiation source of greatest concern, because it is responsible for the major radiation damages in ceramic waste forms, such as radiation-induced amorphization and phase separation that have direct impact on the retention of the incorporated radionuclides, especially the highly mobile I-129. The 1 MeV Kr^{2+} irradiation was conducted using the IVEM-Tandem facility at Argonne National Laboratory, which combines a Hitachi H-9000NAR transmission electron microscope (TEM) with ion accelerators to allow *in situ* TEM observation of the radiation damage process. The SPS-700C sample was ground and dispersed on a carbon-coated TEM grid, before loaded in the TEM and irradiated by 1 MeV Kr^{2+}, and the radiation-induced phase change was closely monitored by selected area electron diffraction (SAED). During ion irradiations, the TEM electron beam was intentionally turned off to minimize the electron irradiation effects. The BM-300C powder sample was also irradiated and monitored in the same manner for comparison. A TEM heating stage was used for irradiations at elevated temperatures, to obtain the temperature dependence of the radiation-induced amorphization. The Kr^{2+} fluences were converted into the universal displacive radiation damage unit of displacements per atom (dpa) by the SRIM 2008 program using a displacement energy (E_d) of 50 eV for all the atoms, as previously suggested by other studies based on theoretical calculations.[24,26,29]

To simulate the effects of beta decay on iodoapatite, 200 keV, electron irradiations were conducted using the focused electron beam and monitored in the same TEM. Gamma irradiation was conducted on the SPS-densified pellets using the LINAC facility at Rensselaer Polytechnic Institute, where a gamma ray with a continuous energy spectrum in the MeV range was generated by deceleration (Bremsstrahlung) of a 15 MeV electron beam by a metal target,

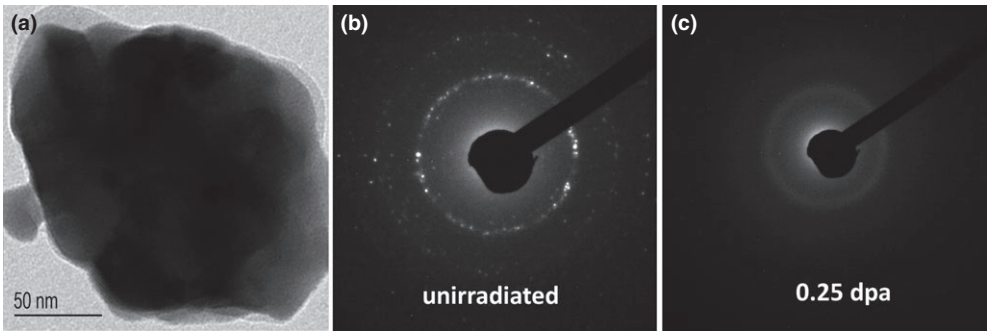

Fig. 1. (a) A bright-field TEM image of the nanocrystalline BM-300C; (b) SAED pattern showing the diffraction rings of the unirradiated BM-300C; (c) SAED pattern showing the amorphous halo of the BM-300C at irradiated by 1 MeV Kr^{2+} to 0.25 dpa at room temperature.

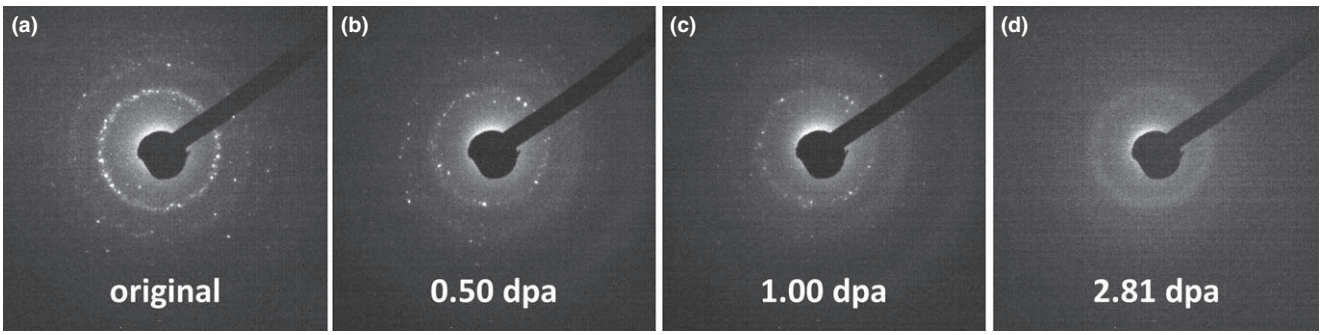

Fig. 2. A sequence of SAED patterns showing the 1 MeV Kr^{2+} irradiation-induced amorphization process of BM-300C at 513 K: (a) unirradiated crystalline sample; (b) 0.50 dpa; (c) 1.00 dpa; (d) complete amorphization at 2.81 dpa.

with doses up to 500 kGy, a level known to cause structural, microstructural and property changes in ceramic nuclear wastes.[30–32] *Ex situ* X-ray diffraction (XRD) and Raman spectroscopy were conducted on the gamma-ray-irradiated iodoapatite samples to determine the radiation effects.

III. Results and Discussion

(1) Ion Irradiation

The highly flexible, open frame structure of apatite allows the incorporation of not only the voluminous I-129, but also various actinides and FPs in the structure to achieve a very high waste loading. When actinides are incorporated, their alpha decay events will cause damage to the apatite host phase mainly through elastic collisions and displacements of the lattice atoms. In extreme cases, under long-term alpha decay irradiations, the originally crystalline apatite waste form can undergo a crystalline-to-amorphous transformation, which may lead to increased migration and eventual release of radionuclide, especially I-129. Such displacive radiation-induced amorphization have been reported in a wide range of ceramic waste forms like monazite,[33,34] pyrochlore,[35,36] garnet,[37,38] and zircon.[34,39] Recent studies have revealed that the radiation tolerance of crystalline ceramics depends on various factors including chemical composition,[26,35] structural ordering,[40] grain size,[33,41] and radiation condition.[22,42] The purpose of the 1 MeV Kr^{2+} irradiation experiments is to investigate the radiation stability of the SPS-consolidated iodoapatite samples and determine the underlying factor that contributes to the radiation tolerance. The two iodoapatite sample types of BM-300C and SPS-700C were irradiated at different temperatures and the data were compared, to determine the effect of SPS on the radiation stability of iodoapatite.

Under 1 MeV Kr^{2+} irradiation at room temperature, BM-300C underwent a radiation-induced amorphization as the irradiation dose reached a critical dose (D_c) of 0.25 dpa (1×10^{14} ions/cm^2). As shown in the SAED patterns in Figs. 1(b) and (c), before irradiation, the SAED pattern of BM-300C shows clear diffraction rings from the 30–50-nm-sized nanocrystalline particles [Fig. 1(b)]; at 0.25 dpa, the diffraction rings completely disappeared and the diffuse halo appeared [Fig. 1(c)], indicating a completely amorphous state. At elevated temperature, the BM-300C exhibits significant defect annealing, such that the D_c increased dramatically when the temperature exceeded 500 K (227°C). Figure 2 shows a sequence of SAED patterns taken at different irradiation doses at 513 K (240°C), in which the clear diffraction rings from the unirradiated sample [Fig. 2(a)] gradually dimmed upon increasing dose until they were completely replaced by the amorphous halo at a D_c of 2.81 dpa [Figs. 2(b)–(d)], 10 times higher than that at room temperature. The temperature dependence of the critical amorphization dose D_c as shown in Fig. 3 was fit and plotted based on a direct-impact-model-based empirical exponential equation:[39,43]

$$D_c = \frac{D_0}{1 - \exp\left[\left(\frac{E_a}{k}\right)\left(\frac{1}{T_c} - \frac{1}{T}\right)\right]}$$

where D_0 is the critical amorphization dose extrapolated at $T = 0$ K, E_a is the activation energy for defect annealing, and T_c is the critical amorphization temperature. The physical meaning of T_c is the upper temperature limit for the radiation-induced amorphization to occur. When the temperature exceeds T_c, all of the defects induced by irradiation can be annealed such that complete amorphization cannot occur. Therefore, T_c can also be used to indicate the radiation tolerance of materials, of which a lower T_c usually implies higher defect annealing capabilities at elevated temperatures and hence greater tolerance against radiation-induced amorphization. The temperature dependence curve of D_c for the BM-300C sample is plotted in Fig. 3, and its T_c is determined as 515 K. This T_c is confirmed by irradiation experiment conducted at 523 K, merely 8 K higher than the T_c, in which no complete amorphization was observed even at a high dose of 6.25 dpa.

The lead vanadate iodoapatite $Pb_{9.85}(VO_4)_6I_{1.7}$ BM-300C exhibits significantly higher radiation tolerance than the previously reported isostructural calcium and lead vanadate fluorapatite $(Pb_xCa_{1-x})_{10}(VO_4)_6F_2$.[26] As a comparison, the temperature dependence curve of D_c of calcium vanadate fluorapatite $Ca_{10}(VO_4)_6F_2$ is also plotted in Fig. 3, showing a lower room temperature D_c of 0.21 dpa and a higher T_c of 603 K. As the radiation tolerance of $(Pb_xCa_{1-x})_{10}(VO_4)_6F_2$ decreases with increasing Pb content,[26] it is apparent that

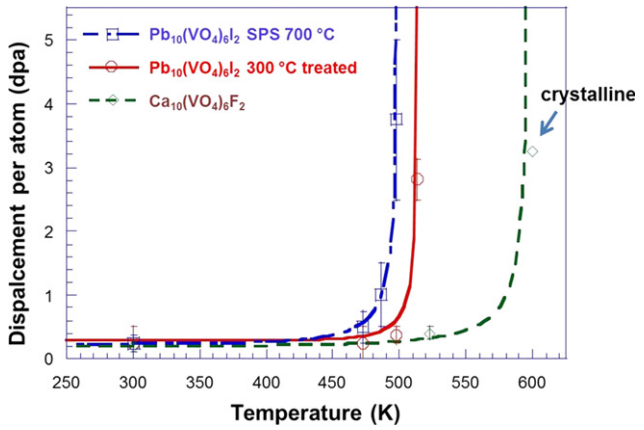

Fig. 3. Temperature dependence curves of D_c for SPS-700C, BM-300C and the previously reported $Ca_{10}(VO_4)_6F_2$[26] showing a decreasing radiation tolerance from left to right. The open diamond on the far right side indicates that $Ca_{10}(VO_4)_6F_2$ is still crystalline at this point.

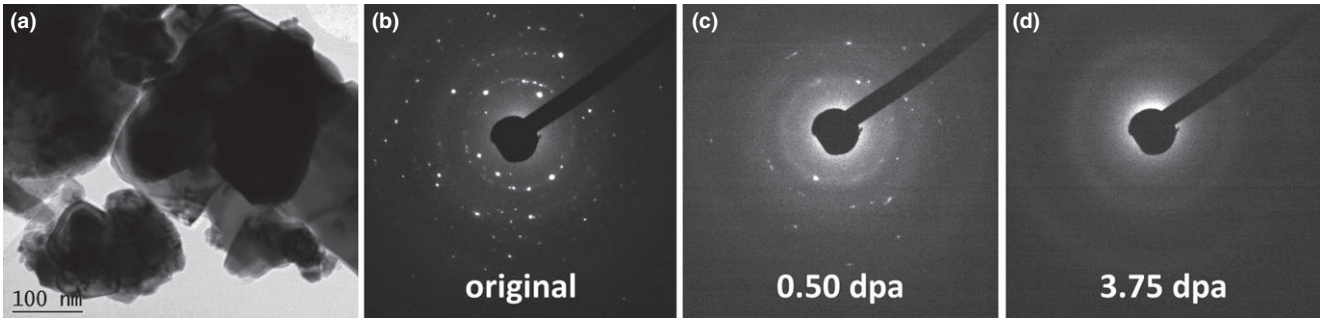

Fig. 4. (a) A bright TEM image of powders mechanically ground from dense SPS-700C; (b–d) sequence of SAED patterns showing the 1 MeV Kr^{2+} irradiation-induced amorphization of SPS-700C at 498 K: (b) unirradiated crystalline SPS-700C, (c) SPS-700C irradiated to 0.50 dpa; (d) complete amorphization of SPS-700C at 3.75 dpa.

lead vanadate iodoapatite $Pb_{9.85}(VO_4)_6I_{1.7}$ is much more radiation tolerant than lead vanadate fluorapatite $Pb_{10}(VO_4)_6F_2$, and the radiation tolerance order is $Pb_{9.85}(VO_4)_6I_{1.7} > Ca_{10}(VO_4)_6F_2 > Pb_{10}(VO_4)_6F_2$. The higher radiation tolerance of iodoapatite than fluorapatite may be attributed to difference in energy loss upon energetic charge particle interaction. The energy loss of the incident ions is mainly due to two mechanisms: the ballistic effect of nuclear energy loss or nuclear stopping power (S_n) which can cause atomic displacements and consequently amorphization of the irradiated crystalline ceramics, and the electronic energy loss or electronic stopping power (S_e), of which a moderate value may benefit the defect recovery process and enhance the radiation tolerance.[44–46] Therefore, higher ratios of electronic-to-nuclear stopping power (ENSP) may result in higher radiation tolerance. The substitution of iodine for fluorine in the anionic position of apatite leads to a higher ENSP (0.626 vs. 0.613) as estimated by the SRIM-2008 program, which may explain the higher radiation stability occurred in iodoapatite.

The SPS-densification process resulted in improved crystallinity, dense microstructure and a significant grain growth in iodoapatite. The grain size grew from below 10 nm in BM-300C to hundreds of nm or microns in SPS-700C, as shown in Fig. 4(a). SPS-700C also exhibits even higher radiation tolerance than BM-300C. At room temperature, radiation-induced amorphization occurred at 0.25 dpa in SPS-700C, similar to that in BM-300C. However, at elevated temperature, the D_c of SPS-700C increases more dramatically than BM-300C. At 498 K, SPS-700C was not completely amorphized until the dose reached 3.75 dpa, as evidenced by the sequence of SAED patterns taken at different doses in Figs. 4(b)–(d). The irradiation experiments were also carried out at elevated temperatures to obtain a set of D_c data points used to generate a temperature dependence curve plotted in Fig. 3. The T_c of SPS-700C is 502 K, lower than that of BM-300C. A comparison of the radiation response of SPS-700C iodoapatite, BM-300C iodoapatite, $Ca_{10}(VO_4)_6F_2$, and $Pb_{10}(VO_4)_6F_2$ is given in Fig. 3, indicating the radiation stability in the order of SPS-700C > BM-300C > $Ca_{10}(VO_4)_6F_2 > Pb_{10}(VO_4)_6F_2$. Further enhancement in the radiation tolerance by SPS is likely attributed to improved crystallinity and structural ordering in the iodoapatite by high-temperature sintering and SPS rapid consolidation.

(2) Electron and Gamma Irradiations

The 200 keV electron beam irradiation was used to simulate the beta decay events associated with the incorporated I-129 and other FPs. As compared to 1 MeV Kr^{2+}, the 200 keV electrons are much less likely to cause atomic displacement cascades in iodoapatite, as the energy is mostly lost to electronic stopping power S_e and ionization in the materials. In some cases, the electron beam irradiation can assist the defect recovery and even facilitate the crystallization and grain growth of displacive-radiation-damaged materials.[24,33,44] *In situ* TEM observation confirmed that no significant amorphization, phase change or major microstructural damage occurred in the electron beam irradiated BM-300C and SPS-700C TEM samples.

The effects of gamma ray emission on the iodoapatite waste form were investigated by gamma ray irradiation of SPS-700C to different dose levels of 50, 100, and 500 kGy. *Ex situ* XRD patterns of the irradiated SPS-700C showed very little changes even at the highest dose of 500 kGy, indicating that the crystal structure of iodoapatite remained the same. However, Raman spectroscopic analysis revealed subtle changes in the chemical bonding of iodoapatite upon gamma irradiation. Raman spectra of the original and irradiated samples are shown in Fig. 5(a), in which significant changes are found in two regions: one in the higher wave number range 750–850 cm^{-1} associated with the stretching vibration of VO_4 tetrahedra [Fig. 5(b)], and the other in the lower wave number range 300–400 cm^{-1} associated with the bending of the O–V–O bond [Fig. 5(c)].[47] In Fig. 5(b), the original sample shows the strongest peak centered around 813 cm^{-1}, which is attributed to the A_g symmetric stretching mode of the VO_4 tetrahedra. The E_{2g} asymmetric stretching vibrational peak at 776 cm^{-1} is abnormally low as compared to those previously reported.[47–49] Upon gamma irradiation,

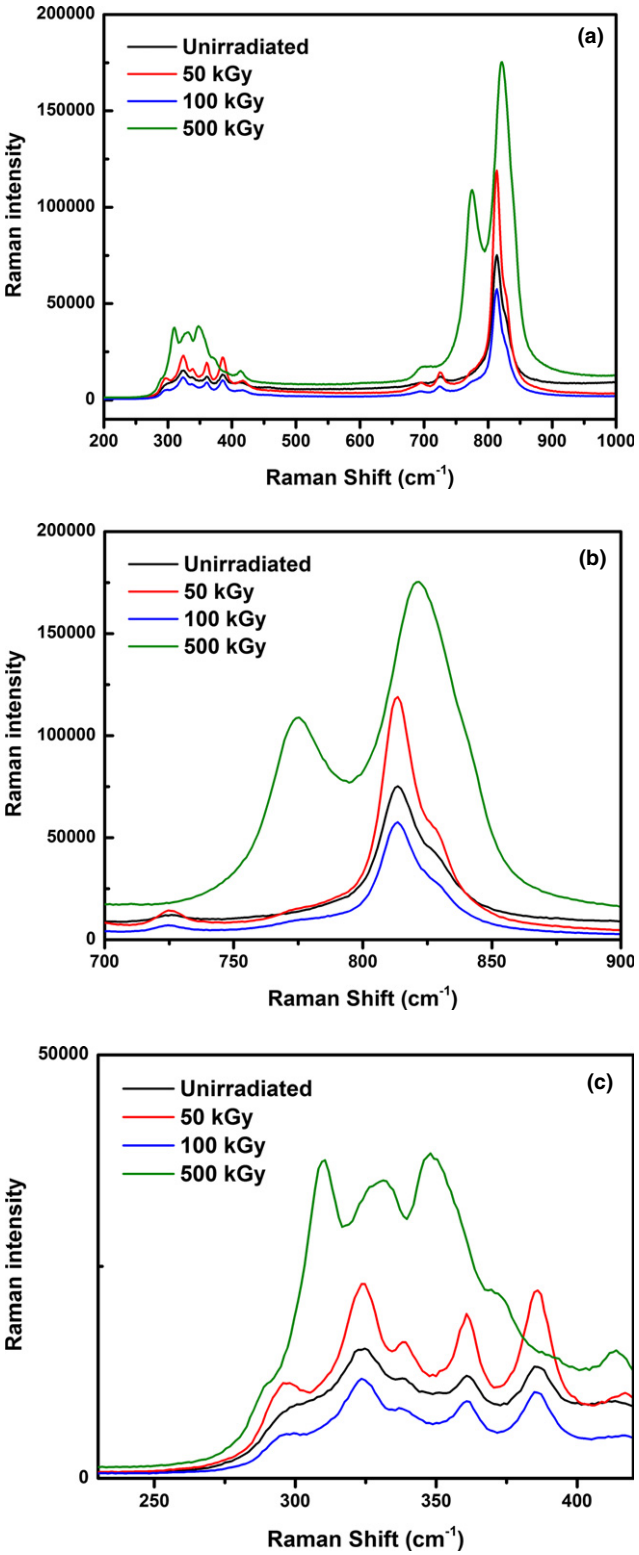

Fig. 5. Raman spectra of the unirradiated SPS-700C and samples irradiated with 50, 100, and 500 kGy gamma ray: (a) overall wave number range 200–1000 cm^{-1}; (b) higher wave number range 750–850 cm^{-1}; (c) lower wave number range 300–400 cm^{-1}.

the changes in the VO_4 stretching modes remained insignificant until the dose reached 500 kGy, when the E_{2g} asymmetric stretching peak at 776 cm^{-1} showed a remarkable increase in intensity by two times, and the A_g symmetric stretching mode shifted from 813 cm^{-1} to a higher wave number of 823 cm^{-1}. By adopting the empirical method presented by Hardcastle and Wachs,[50] the changes in V–O bond length and bond strength of iodoapatite at the highest gamma ray dose can be related to the shifting of the A_g stretching frequency, and their values were estimated by using the following empirical functions. The bond length R is given in

$$\nu = 21349\exp(-1.9176R)$$

and the bond strength s(V–O) is given by

$$s(V-O) = \left[0.2912\ln\left(\frac{21349}{\nu}\right)\right]^{-5.1}$$

where ν is the vibrational frequency. As the A_g stretching mode shifted from 813 to 823 cm^{-1}, the V–O bond length decreased from 1.704 to 1.698 Å, and the bond strength increased from 1.2876 to 1.3124 vu (vu is the valence unit). As the bond strength indicates the bond order, the vibration frequency shift implies improved iodoapatite V–O bond order upon gamma irradiation. In the lower wave number range in Fig. 5(c), vibrational bands at ~305, 330, and 350 cm^{-1} corresponding to the asymmetric O–V–O bending vibrational modes emerged at the highest dose of 500 kGy. All these changes in the Raman spectra point to a more ordered bonding structure in gamma-irradiated vanadate iodoapatite, which suggests that high dose gamma irradiation may improve the V–O bond order in the SPS-700C sample.

Generally, the systematic ion, electron and gamma irradiations indicate excellent radiation stability of the SPS-densified iodoapatite used as a nuclear waste form. Under displacive 1 MeV Kr^{2+} irradiation, iodoapatite exhibits a T_c lower than many types of apatites,[26,36] garnet,[37] pyrochlores,[35] and zircons[51] proposed as nuclear waste forms, implying great defect annealing at elevated temperatures. Furthermore, the SPS processing further enhances the radiation tolerance of iodoapatite and reduces the T_c from 515 K in BM-300C to 502 K in SPS-700C. Therefore, other than an effective consolidation and densification technique for the fabrication of iodine-bearing ceramic waste forms, SPS also has the advantage of improving the radiation tolerance against alpha-decay-induced amorphization. The electron irradiations show insignificant effects of beta decay events on the phase and microstructure of iodoapatite. Intense gamma irradiation dose may enhance the V–O bond order in the SPS-densified iodoapatite, probably due to an ionization-assisted process. Overall, the spark-plasma-sintered iodoapatite is a promising waste form that can remain stable under complex radiation conditions in the long term.

IV. Conclusions

Systematic irradiations of the SPS-densified lead vanadate iodoapatite were conducted to investigate its radiation stability in the presence of different radiation sources of alpha-, beta-, and gamma decays. The experimental results generally indicate excellent radiation stability of the iodoapatite. Under energetic ion irradiations, the SPS-700C iodoapatite shows enhanced tolerance against radiation-induced amorphization, as compared with as-milled lead vanadate iodoapatite, conventionally synthesized lead vanadate fluorapatite, and many other types of ceramic waste forms. The enhanced radiation performance for the SPS-densified iodoapatite may be attributed to the improved crystallinity and dense microstructure. In addition, the SPS-densified pellet is also largely stable under beta irradiation and even shows improved bond ordering under intense gamma rays. Owing to its radiation stability, the SPS-densified iodoapatite holds great promise for the immobilization and disposal of I-129.

Acknowledgments

This work is supported by DOE NEUP (Nuclear Engineering University Program) under the award DE-AC07-05ID14517. JL also acknowledges a NSF career award DMR 1151028 in the synthesis of iodoapatite by high energy ball milling and consolidation by spark plasma sintering. FL acknowledges the support of the U.S. Nuclear Regulatory Commission Faculty Development Grant (NRC-38-10-933). The authors also thank the staff of the IVEM-tandem facility at the Argonne National Laboratory and the staff of the LINAC facility at Rensselaer Polytechnic Institute for their assistance with the irradiation experiments.

References

[1]F. Audubert, J. Carpena, J. L. Lacout, and F. Tetard, "Elaboration of an Iodine-Bearing Apatite - Iodine Diffusion into a $Pb_3(VO_4)_2$ Matrix," *Solid State Ionics*, **95** [1–2] 113–9 (1997).

[2]R. C. Ewing, "Nuclear Waste Forms for Actinides," *P. Natl. Acad. Sci. USA*, **96** [7] 3432–9 (1999).

[3]R. C. Ewing, "The Design and Evaluation of Nuclear-Waste Forms: Clues from Mineralogy," *Can. Miner.*, **39**, 697–715 (2001).

[4]S. Le Gallet, et al., "Spark Plasma Sintering of Iodine-Bearing Apatite," *J. Nucl. Mater.*, **400** [3] 251–6 (2010).

[5]L. Merker and H. Wondratschek, "Bleiverbindungen Mit Apatitstruktur, Insbesondere Blei Jod-Apatite Und Blei Brom-Apatite," *Z. Anorg. Allg. Chem.*, **300** [1–2] 41–50 (1959).

[6]M. C. Stennett, I. J. Pinnock, and N. C. Hyatt, "Rapid Synthesis of $Pb_5(VO_4)_3I$, for the Immobilisation of Iodine Radioisotopes, by Microwave Dielectric Heating," *J. Nucl. Mater.*, **414** [3] 352–9 (2011).

[7]N. Gmati, K. Boughzala, A. Chaabene, N. Fattah, and K. Bouzouita, "Mechanochemical Synthesis of Strontium Apatites Doped with Lanthanum and Cesium," *Cr. Chim.*, **16** [8] 712–20 (2013).

[8]S. P. Kumar and G. Buvaneswari, "Synthesis of Apatite Phosphates Containing Cs^+, Sr^{2+} and RE^{3+} Ions and Chemical Durability Studies," *Mater. Res. Bull.*, **48** [2] 324–32 (2013).

[9]C. Gaillard, C. Den Auwer, and S. D. Conradson, "An X-ray Absorption Near Edge Spectroscopy Study of Trace Amount Technetium Implanted in Apatite," *Phys. Chem. Chem. Phys.*, **4** [12] 2499–500 (2002).

[10]R. El Ouenzerfi, M. T. Cohen-Adad, C. Goutaudier, and G. Panczer, "Uranium-Doped Britholites $Ca_xLa_y(SiO_4)_{6-u}(PO_4)_uO_t$: U Synthesis, Characterization and Preliminary Study of Uranium Diffusion," *Solid State Ionics*, **176** [1–2] 225–31 (2005).

[11]V. Natarajan, T. K. Seshagiri, R. Veeraraghavan, and M. D. Sastry, "Radiation Effects in Plutonium and Carbonate co-Doped Calcium Hydroxy Apatite: An EPR Study," *J. Radioanal. Nucl. Ch.*, **256** [3] 445–9 (2003).

[12]K. Popa, et al., "Thermodynamic Properties of $CaTh(PO_4)_2$ Synthetic Cheralite," *Am. Miner.*, **93** [8–9] 1356–62 (2008).

[13]J. Rakovan, R. J. Reeder, E. J. Elzinga, D. J. Cherniak, C. D. Tait, and D. E. Morris, "Structural Characterization of U(VI) in Apatite by X-ray Absorption Spectroscopy," *Environ. Sci. Technol.*, **36** [14] 3114–7 (2002).

[14]O. Terra, F. Audubert, N. Dacheux, C. Guy, and R. Podor, "Synthesis and Characterization of Uranium-Bearing Britholites," *J. Nucl. Mater.*, **366** [1–2] 70–86 (2007).

[15]F. Goubard, P. Griesmar, and A. Tabuteau, "Alpha Self-Irradiation Effects in Ternary Oxides of Actinides Elements: The Zircon-Like Phases $Am^{III}VO_4$ and $A^{II}Np^{IV}(VO_4)_2$ (A = Sr, Pb)," *J. Solid State Chem.*, **178** [6] 1898–902 (2005).

[16]F. Y. Lu, et al., "Facile Low Temperature Solid State Synthesis of Iodoapatite by High-Energy Ball Milling," *Rsc. Adv.*, **4** [73] 38718–25 (2014).

[17]T. K. Yao, F. Y. Lu, H. T. Sun, J. W. Wang, R. C. Ewing, and J. Lian, "Bulk Iodoapatite Ceramic Densified by Spark Plasma Sintering with Exceptional Thermal Stability," *J. Am. Ceram. Soc.*, **97** [8] 2409–12 (2014).

[18]C. Guy, F. Audubert, J. E. Lartigue, C. Latrille, T. Advocat, and C. Fillet, "New Conditionings for Separated Long-Lived Radionuclides," *C.R. Phys.*, **3** [7–8] 827–37 (2002).

[19]M. Uno, M. Shinohara, K. Kurosaki, and S. Yamanaka, "Some Properties of a Lead Vanado-Iodoapatite $Pb_{10}(VO_4)_6I_2$," *J. Nucl. Mater.*, **294** [1–2] 119–22 (2001).

[20]W. J. Weber, et al., "Radiation Effects in Crystalline Ceramics for the Immobilization of High-Level Nuclear Waste and Plutonium," *J. Mater. Res.*, **13** [6] 1434–84 (1998).

[21]A. Meldrum, L. M. Wang, and R. C. Ewing, "Electron-Irradiation-Induced Phase Segregation in Crystalline and Amorphous Apatite: A TEM Study," *Am. Miner.*, **82** [9–10] 858–69 (1997).

[22]S. Utsunomiya, S. Yudintsev, L. M. Wang, and R. C. Ewing, "Ion-Beam and Electron-Beam Irradiation of Synthetic Britholite," *J. Nucl. Mater.*, **322** [2–3] 180–8 (2003).

[23]L. M. Wang and W. J. Weber, "Transmission Electron Microscopy Study of Ion-Beam-Induced Amorphization of $Ca_2La_8(SiO_4)_6O_2$," *Philos. Mag. A*, **79** [1] 237–53 (1999).

[24]W. J. Weber, Y. W. Zhang, H. Y. Xiao, and L. M. Wang, "Dynamic Recovery in Silicate-Apatite Structures Under Irradiation and Implications for Long-Term Immobilization of Actinides," *Rsc. Adv.*, **2** [2] 595–604 (2012).

[25]S. Soulet, J. Carpena, J. Chaumont, O. Kaitasov, M. O. Ruault, and J. C. Krupa, "Simulation of the Alpha-Annealing Effect in Apatitic Structures by He-Ion Irradiation: Influence of the Silicate/Phosphate Ratio and of the OH^-/F^- Substitution," *Nucl. Instrum. Meth. B*, **184** [3] 383–90 (2001).

[26]F. Y. Lu, Z. L. Dong, J. M. Zhang, T. White, R. C. Ewing, and J. Lian, "Tailoring the Radiation Tolerance of Vanadate-Phosphate Fluorapatites by Chemical Composition Control," *Rsc. Adv.*, **3** [35] 15178–84 (2013).

[27]S. Miro, et al., "X-ray Diffraction Study of Damage Induced by Swift Heavy Ion Irradiation in Fluorapatite," *Nucl. Instrum. Meth. B*, **227** [3] 306–18 (2005).

[28]S. A. T. Redfern, S. E. Smith, and E. R. Maddrell, "High-Temperature Breakdown of the Synthetic Iodine Analogue of Vanadinite, $Pb_5(VO_4)_3I$: An Apatite-Related Compound for Iodine Radioisotope Immobilization?" *Miner. Mag.*, **76** [4] 997–1003 (2012).

[29]C. Meis, "Computational Study of Plutonium-Neodymium Fluorobritholite $Ca_9Nd_{0.5}Pu_{0.5}(SiO_4)(PO_4)_5F_2$ Thermodynamic Properties and Threshold Displacement Energies," *J. Nucl. Mater.*, **289** [1–2] 167–76 (2001).

[30]S. Baccaro, N. Catallo, A. Cemmi, and G. Sharma, "Radiation Damage of Alkali Borate Glasses for Application in Safe Nuclear Waste Disposal," *Nucl. Instrum. Meth. B*, **269** [2] 167–73 (2011).

[31]N. Deng, et al., "Effects of Gamma-Ray Irradiation on Leaching of Simulated $^{133}Cs^+$ Radionuclides from Geopolymer Wasteforms," *J. Nucl. Mater.*, **459**, 270–5 (2015).

[32]C. Jegou, et al., "Effect of External Gamma Irradiation on Dissolution of the Spent UO_2 Fuel Matrix," *J. Nucl. Mater.*, **341** [1] 62–82 (2005).

[33]F. Y. Lu, Y. Q. Shen, X. Sun, Z. L. Dong, R. C. Ewing, and J. Lian, "Size Dependence of Radiation-Induced Amorphization and Recrystallization of Synthetic Nanostructured $CePO_4$ Monazite," *Acta Mater.*, **61** [8] 2984–92 (2013).

[34]A. Meldrum, L. A. Boatner, and R. C. Ewing, "Displacive Radiation Effects in the Monazite- and Zircon-Structure Orthophosphates," *Phys. Rev. B*, **56** [21] 13805–14 (1997).

[35]J. Lian, et al., "Radiation-Induced Amorphization of Rare-Earth Titanate Pyrochlores," *Phys. Rev. B*, **68** [1] 3 (2003).

[36]S. X. Wang, B. D. Begg, L. M. Wang, R. C. Ewing, W. J. Weber, and K. V. G. Kutty, "Radiation Stability of Gadolinium Zirconate: A Waste Form for Plutonium Disposition," *J. Mater. Res.*, **14** [12] 4470–3 (1999).

[37]J. M. Zhang, T. S. Livshits, A. A. Lizin, Q. N. Hu, and R. C. Ewing, "Irradiation of Synthetic Garnet by Heavy Ions and Alpha-Decay of Cm-244," *J. Nucl. Mater.*, **407** [3] 137–42 (2010).

[38]S. Utsunomiya, L. M. Wang, S. Yudintsev, and R. C. Ewing, "Ion Irradiation-Induced Amorphization and Nano-Crystal Formation in Garnets," *J. Nucl. Mater.*, **303** [2–3] 177–87 (2002).

[39]W. J. Weber, R. C. Ewing, and L. M. Wang, "The Radiation-Induced Crystalline-to-Amorphous Transition in Zircon," *J. Mater. Res.*, **9** [3] 688–98 (1994).

[40]J. M. Zhang, et al., "Enhanced Radiation Resistance of Nanocrystalline Pyrochlore $Gd_2(Ti_{0.65}Zr_{0.35})_2O_7$," *Appl. Phys. Lett.*, **94** [24] 243110 (2009).

[41]T. D. Shen, S. Feng, M. Tang, J. A. Valdez, Y. Wang, and K. E. Sickafus, "Enhanced Radiation Tolerance in Nanocrystalline $MgGa_2O_4$," *Appl. Phys. Lett.*, **90** [26] 263115 (2007).

[42]F. Y. Lu, et al., "Amorphization of Nanocrystalline Monoclinic ZrO_2 by Swift Heavy Ion Irradiation," *Phys. Chem. Chem. Phys.*, **14** [35] 12295–300 (2012).

[43]S. X. Wang, L. M. Wang, and R. C. Ewing, "Irradiation-Induced Amorphization: Effects of Temperature, Ion Mass, Cascade Size, and Dose Rate," *Phys. Rev. B*, **63** [2] 024105 (2001).

[44]F. Y. Lu, J. M. Zhang, M. B. Huang, F. Namavar, R. C. Ewing, and J. Lian, "Phase Transformation of Nanosized ZrO_2 Upon Thermal Annealing and Intense Radiation," *J. Phys. Chem. C*, **115** [15] 7193–201 (2011).

[45]A. Meldrum, L. A. Boatner, and R. C. Ewing, "Electron-Irradiation-Induced Nucleation and Growth in Amorphous $LaPO_4$, $ScPO_4$, and Zircon," *J. Mater. Res.*, **12** [7] 1816–27 (1997).

[46]W. J. Weber, Y. W. Zhang, and L. M. Wang, "Review of Dynamic Recovery Effects on Ion Irradiation Damage in Ionic-Covalent Materials," *Nucl. Instrum. Meth. B*, **277**, 1–5 (2012).

[47]R. L. Frost, M. Crane, P. A. Williams, and J. T. Kloprogge, "Isomorphic Substitution in Vanadinite $[Pb_5(VO_4)_3Cl]$ - a Raman Spectroscopic Study," *J. Raman Spectrosc.*, **34** [3] 214–20 (2003).

[48]J. G. Eon, C. B. Boechat, A. M. Rossi, J. Terra, and D. E. Ellis, "A Structural Analysis of Lead Hydroxyvanadinite," *Phys. Chem. Chem. Phys.*, **8** [15] 1845–51 (2006).

[49]Q. He, X. Liu, X. M. Hu, S. C. Li, and H. J. Wang, "Solid Solution Between Lead Fluorapatite and Lead Fluorvanadate Apatite: Mixing Behavior, Raman Feature and Thermal Expansivity," *Phys. Chem. Miner.*, **38** [10] 741–52 (2011).

[50]F. D. Hardcastle and I. E. Wachs, "Determination of Vanadium Oxygen Bond Distances and Bond Orders by Raman-Spectroscopy," *J. Phys. Chem.-Us*, **95** [13] 5031–41 (1991).

[51]A. Meldrum, S. J. Zinkle, L. A. Boatner, and R. C. Ewing, "Heavy-Ion Irradiation Effects in the ABO_4 Orthosilicates: Decomposition, Amorphization, and Recrystallization," *Phys. Rev. B*, **59** [6] 3981–92 (1999). □